Received: 6 August 2021 | Revised: 7 September 2021 | Accepted: 13 September 2021

DOI: 10.1002/aoc.6469

Applied Organometallic Chemistry WILEY

FULL PAPER

WELPSA: A natural catalyst of alkali and alkaline earth metals for the facile synthesis of tetrahydrobenzo[*b*]pyrans and pyrano[2,3-*d*]pyrimidinones as inhibitors of SARS-CoV-2

Aravind R. Nesaragi[1] | **Ravindra R. Kamble**[1] | **Swati R. Hoolageri**[1] | **Ahmedraza Mavazzan**[1] | **Suresh F. Madar**[1] | **Ashish Anand**[2] | **Shrinivas D. Joshi**[3]

[1]Department of Studies in Chemistry, Karnatak University Dharwad, Dharwad, India

[2]Solid State and Structural Chemistry Unit, Indian Institute of Science, Bengaluru, India

[3]Novel Drug Design and Discovery Laboratory, Department of Pharmaceutical Chemistry, S.E.T.'s College of Pharmacy, Dharwad, India

Correspondence
Ravindra R. Kamble, Department of Studies in Chemistry, Karnatak University Dharwad, Dharwad 580003, India.
Email: ravichem@kud.ac.in

Since 2019, the infection of SARS-CoV-2 has been spreading worldwide and caused potentially lethal health problems. In view of this, the present study explores the most commodious and environmentally benign synthetic protocol for the synthesis of tetrahydrobenzo[*b*]pyran and pyrano[2,3-*d*] pyrimidinones as SARS-CoV-2 inhibitors via three-component cycloaddition of aromatic aldehyde, malononitrile, and dimedone/barbituric acid in water. Lemon peel from juice factory waste, namely, lemon (*Citrus limon*), sweet lemon (*C. limetta*), and Kaffir lime or Citron (*C. hystrix*), effectually utilized to obtain WELPSA, WESLPSA, and WEKLPSA, respectively, for the synthesis of title compounds. The catalyst was characterized by scanning electron microscope (SEM) and energy-dispersive x-ray spectroscopy (EDX). The concentration of sodium, potassium, calcium, and magnesium in the catalyst (WELPSA) was determined using atomic absorption spectrometry (AAS). The current approach manifests numerous notable advantages that include ease of preparation, handling and benignity of the catalyst, low cost, green reaction conditions, facile workup, excellent yields (93%–97%) with extreme purity, and recyclability of the catalyst. Compounds were docked on the crystal structure of SARS-CoV-2 (PDB: 6M3M). The consensus score obtained in the range 2.47–4.63 suggests that docking study was optimistic indicating the summary of all forces of interaction between ligands and the protein.

KEYWORDS

atomic absorption spectrometry, Covid-19, pyrano[2,3-*d*]pyrimidinones, tetrahydrobenzo[*b*]pyrans, WELPSA

1 | INTRODUCTION

Coronavirus has become the lethal pandemic of 21st century and emphasizes the role of viruses in contagious diseases. It has caused a critical onset of deadly pneumonia, instigated by the severe acute respiratory syndrome coronavirus (SARS-CoV). The SARS-CoV-2 has affected more than 213 countries around the world with more than 190 million confirmed cases and more than 4.1 million confirmed deaths.[1] Unlike SARS-CoV and MERS-CoV (Middle East respiratory syndrome coronavirus), SARS-CoV-2 fits into the betacoronavirus (beta-CoV) ancestry, RNA viruses with crown-like thorns over the superficial of the coronavirus particles. Nevertheless, SARS-CoV-2 has characteristics like instant transmission among people, asymptomatic spread, and extended symptomatic growth together with significantly increased deaths.[2]

Many antiviral drugs were under trial in the initial stages of the pandemic, and the recently developed vaccines are thought to avoid the attack of coronavirus when a person is been vaccinated. But contradictory to it, many people who have been vaccinated also being caught by this infection and are suffering. More than 213 countries that have been influenced by coronavirus are facing lockdown so as to avoid the gathering of people affected economically as well. The governments conflict with new lockdown extents to tackle the extension of the virus as the propagation of deadly virus has left national economies and businesses counting the costs. The global shares are in flux, world economies struggling with rising unemployment, new vacancies are still very low in many countries, majority of countries in recession, commercial flights remain well below normal levels, the global tourism industry is crumbling. The only positive development came up with the pandemic is the rise of pharmaceutical companies which is contradictory.[3] Despite the development of new vaccines, the pandemic still remains the deadliest viral infection.

We have listed out the Top 10 countries in the world that have been most affected by the Covid pandemic (Table 1).[4] The data consist of number of corona waves the country has been going through, total number of cases, deaths and average cases/day.

Structure-based virtual screening method is a rapid and noteworthy approach for recognizing inhibitor molecules targeting SARS-CoV-2.[5] Protein and ligand interactions play a vital part, wherein the latter is accountable for limiting/curtailing the activity of the earlier in many human cellular and biological functions. SARS-CoV-2 is an essential drug target, and computer-aided drug design (CADD) is deemed as an undeniable and noteworthy strategy to ascertain antiviral drug candidates.[6] In this article, we intend to execute a fast innovation of the prospective candidates against SARS-CoV-2 through virtual screening protocol and build a focused library of novel potential compounds. We have developed a green synthetic protocol to afford tetrahydrobenzo[*b*]pyran and pyrano[2,3-*d*]pyrimidinones and carried out their molecular docking studies on the crystal structure of SARS-CoV-2 nucleocapsid protein N-terminal RNA binding domain (PDB ID 6M3M, 2.70 Å x-ray diffraction).

Recently, it has become the constraint for a synthetic chemist to provide a meritorious, proficient, user-friendly, and environmentally benign synthetic protocol in organic synthesis. Efforts are underway to curtail the malignant levels of catalysts by multidirectional amendments driving to the advancement of organic reactions underneath the catalysts designed from the agro- and agricultural product-related wastes.[7] Therefore, conception and advancement of such natural catalyst reactions have acquired enormous consideration within the range of green organic synthesis. Multicomponent reactions (MCRs) in aqueous media with such catalysts are exceedingly alluring the tools of green chemistry.[8] The diminution of by-products by means of straightforward synthesis of complex molecules exclusive of the segregation of the

TABLE 1 Most affected countries due to coronavirus

Country	Total cases (in millions)	Average cases/day	Total deaths (in millions)	Number of waves
United States	35.2	85,866	0.613	3
India	31.77	40,794	0.425	3
Brazil	20	35,120	0.557	3
Russia	6.23	511,265	0.157	3
France	6.15	22,289	0.112	3
United Kingdom	5.9	25,722	0.130	3
Turkey	5.77	22,083	0.052	3
Argentina	4.95	11,183	0.106	2
Colombia	4.8	81,658	0.121	3
Spain	4.5	22,990	0.082	4

intermediates makes MCRs an imperative tactic in organic synthesis over multistep reactions also owing to the constitution of numerous new bonds in a single process.[9]

Intellectual as well as industrial chemists are constantly striving to figure out the adequate sustainable replacements for expensive, toxic, hazardous, and environmental damaging catalysts. Thus, there is an invariable necessitate for most advantageous, fruitful, and eco-friendly catalysts. Owing to the promising health benefits of lemon (*Citrus limon*), sweet lemon (*C. lemitta*), and Kaffir lime (*C. hystrix*), we intend to make the most use of them by synthesizing pyran-based heterocycles. In this paper, we present the natural catalysts WELPSA (water extract of lemon peel soaked ash), WESLPSA (water extract of sweet lemon peel soaked ash) and WEKLPSA (water extract of Kaffir lime peel soaked ash). The pH of the ash extract of lemon was found to be around 12.00–12.02, and this extremely basic nature is one of the important factors in the condensation and cyclization of the reactants to yield final compounds through *Knoevenagel* condensation.

Considerable attention has been attracted on the synthesis, reactions, and biological activities of 4*H*-pyran frameworks such as tetrahydrobenzo[*b*]pyran and pyrano[2,3-*d*]pyrimidinone/thiones owing to their broad spectrum of pharmaceutical and biological properties such as antidiabetic, antimicrobial, antioxidant, antifungal, anti-HIV, antihypertensive, anti-inflammatory, anti-allergic, cytotoxic, and anticancer properties including their utilization in photoactive materials, cosmetics, and pigments.[10–13] Hence, the design and development of novel synthetic methods to similar compounds is an essential area for organic chemists. Amid the recognized protocols for the synthesis of 4*H*-pyran frameworks such as tetrahydrobenzo[*b*]pyran and pyrano[2,3-*d*]pyrimidinone/thiones, the most straightforward method involves a multicomponent protocol of aldehydes, malononitrile, and diverse enolizable C–H activated acidic compounds. Given this, a large number of catalysts were introduced for the three-component synthesis of tetrahydrobenzo[*b*]pyran and pyrano[2,3-*d*]-pyrimidinone/thiones under multifarious catalytic circumstances.[9,14–34] There are numerous catalysts derived from fruit extracts, and agro-wastes have been utilized to synthesize various heterocycles.[35–39]

Even with the essence of such catalysts accompanied by few restrictions such as complexity in synthesizing the catalyst, overpriced reagents, prolonged reaction times, requirement of excessive reagent or catalyst, diminished yields, and tedious workup, we intended in commencing more proficient and user-friendly method by means of scalable green catalyst to accomplish the aforementioned vital target molecules.

2 | EXPERIMENTAL

The reagents used were of analytical grade obtained from commercial suppliers (Sigma-Aldrich, SD Fine, Alfa Aesar, Avra, Spectrochem). Coslab scientific melting point apparatus was utilized to note melting points. Precoated silica gel (Merk 60F-254) plates through which the reaction rates were investigated by thin-layer chromatography (TLC) under UV lamp (λ 254 nm). Infrared spectra (IR) spectra were witnessed on a Nicolet 170 SX FT-IR spectrometer, via potassium bromide (KBr) pellets. JEOL advance NMR spectrometer was used to obtain NMR spectrum and LCMS through Synapt G2 HDMS ACQUITY UPLC. Heraeus Carlo Erba 1180 CHN analyzer was used for elemental analyses (C, H, and N). Single-crystal x-ray investigation was carried out utilizing Bruker SMART CCD area-detector diffractometer with monochromatic Mo Ka radiation at customary temperature.

2.1 | Conventional procedure for the synthesis of tetrahydrobenzo[*b*]pyrans 5a–j and pyrano[2,3-*d*]pyrimidinones 6k–t

A mixture of aromatic aldehyde **1a–j** (0.010 mol), malononitrile **2** (0.010 mol), dimedone **3** (0.010 mol), and WELPSA (3.00 ml) was taken in round-bottom (RB) flask (50 ml) containing water (15.00 ml). The mixture was stirred at room temperature for about 12 h. After completion of the reaction (as monitored by TLC), the precipitated product was filtered off and washed with chilled methanol and recrystallized from ethanol to get the crystals of tetrahydrobenzo[*b*]pyran **5a–j**. Similarly, with the same reaction mixture, barbituric acid **4** (0.010 mol) was used instead of dimedone **3** to obtain the crystals of pyrano[2,3-*d*]pyrimidinone **6k–t**.

2.2 | Microwave-assisted synthesis of tetrahydrobenzo[*b*]pyrans 5a–j and pyrano [2,3-*d*]pyrimidinones 6k–t

A mixture of aromatic aldehyde **1a–j** (0.010 mol), malononitrile **2** (0.010 mol), dimedone **3** (0.010 mol), and WELPSA (3.00 ml) in water (15.00 ml) was taken in a sealed glass vial, and the mixture was irradiated for 3–5 min at 100 W irradiation power and 100°C. The product precipitated out was filtered, washed with chilled

methanol, and recrystallized from ethanol to get pure product of tetrahydrobenzo[*b*]pyran **5a–j**. Similarly, pyrano[2,3-*d*]pyrimidinone **6k–t** was obtained using barbituric acid **4** (0.010 mol) instead of dimedone **3** in the reaction mixture.

2.3 | Spectral characterization of selected compounds

2.3.1 | 2-Amino-5,6,7,8-tetrahydro-7,7-dimethyl-5-oxo-4-phenyl-4*H*-chromene-3-carbonitrile

White solid (yield: 96%); m.p.: 230–232°C; **IR** (KBr, cm^{-1}): 3385 and 3321 (NH_2), 2198 (CN), 1677 (C=O); **^{1}H NMR** (400 MHz, DMSO-d_6) δ (ppm): 0.93 (s, 3H, CH_3), 1.02 (s, 3H, CH_3), 2.08–2.10 (d, $J = 8$ Hz, 2H, CH_2), 2.22–2.24 (d, $J = 8$ Hz, 2H, CH_2), 4.15 (s, 1H, CH), 7.01 (s, 2H, NH_2), 7.09–7.18 (m, 2H, Ar–H), 7.25–7.29 (t, 2H, Ar–H); **^{13}C NMR** (100 MHz, DMSO-d_6) δ (ppm): 27.31, 28.93, 32.35, 36.08, 40.01, 50.47, 58.75, 113.22, 120.29, 127.10, 127.68, 128.87, 145.29, 158.99, 163.04, 196.21; **MS** m/z: 294 (M^+). Elem. anal. calcd for $C_{18}H_{18}N_2O_2$ (%): calcd. C, 73.45; H, 6.16; N, 9.52; found: C, 73.49; H, 6.12; N, 9.50.

2.3.2 | 2-Amino-5,6,7,8-tetrahydro-7,7-dimethyl-5-oxo-4-*p*-tolyl-4*H*-chromene-3-carbonitrile

White solid (yield: 95%); m.p.: 210–212°C; **IR** (KBr, cm^{-1}): 3391 and 3306 (NH_2), 2191 (CN), 1682 (C=O); **^{1}H NMR** (400 MHz, DMSO-d_6) δ (ppm): 1.20 (s, 3H, CH_3), 1.28 (s, 3H, CH_3), 2.14–2.16 (d, $J = 8$ Hz, 2H, CH_2), 2.32 (s, 3H, CH_3), 2.33–2.35 (d, $J = 8$ Hz, 2H, CH_2), 4.37 (s, 1H, CH), 7.23 (s, 2H, NH_2), 7.26–7.28 (d, $J = 8$ Hz, 2H, Ar–H), 7.32–7.34 (d, $J = 8$ Hz, 2H, Ar–H); **^{13}C NMR** (100 MHz, DMSO-d_6) δ (ppm): 21.61, 27.27, 28.95, 32.32, 35.70, 40.02, 50.51, 58.93, 113.38, 120.30, 127.60, 129.40, 136.14, 142.36, 158.95, 162.81, 196.16; **MS** m/z: 308 (M^+). Elem. anal. calcd for $C_{19}H_{20}N_2O_2$ (%): calcd. C, 74.00; H, 6.54; N, 9.08; found: C, 74.03; H, 6.59; N, 9.12.

2.3.3 | 2-Amino-5,6,7,8-tetrahydro-7,7-dimethyl-4-(4-nitrophenyl)-5-oxo-4*H*-chromene-3-carbonitrile

Yellow solid (yield: 96%); m.p.: 184–186°C; **IR** (KBr, cm^{-1}): 3367 and 3305 (NH_2), 2186 (CN), 1680 (C=O); **^{1}H NMR** (400 MHz, DMSO-d_6) δ (ppm): 0.91 (s, 3H, CH_3), 1.00 (s, 3H, CH_3), 2.07–2.09 (d, $J = 8$ Hz, 2H, CH_2), 2.20–2.22 (d, $J = 8$ Hz, 2H, CH_2), 4.33 (s, 1H, CH), 7.16 (s, 2H, NH_2), 7.40–7.42 (d, $J = 8$ Hz, 2H, Ar–H), 8.12–8.14 (d, $J = 8$ Hz, 2H, Ar–H); **^{13}C NMR** (100 MHz, DMSO-d_6) δ (ppm): 27.43, 28.79, 32.36, 36.16, 50.35, 57.45, 112.23, 119.89, 124.22, 129.15, 146.76, 152.83, 159.08, 163.64, 196.25; **MS** m/z: 339 (M^+). Elem. anal. calcd for $C_{18}H_{17}N_3O_4$ (%): calcd. C, 63.71; H, 5.05; N, 12.38; found: C, 63.75; H, 5.09; N, 12.33.

2.3.4 | 2-Amino-4-(4-chlorophenyl)-5,6,7,8-tetrahydro-7,7-dimethyl-5-oxo-4*H*-chromene-3-carbonitrile

White solid (yield: 95%); m.p.: 212–214°C; **IR** (KBr, cm^{-1}): 3379 and 3325 (NH_2), 2188 (CN), 1673 (C=O); **^{1}H NMR** (400 MHz, DMSO-d_6) δ (ppm): 0.94 (s, 3H, CH_3), 1.02 (s, 3H, CH_3), 2.09–2.11 (d, $J = 8$ Hz, 2H, CH_2), 2.28–2.30 (d, $J = 8$ Hz, 2H, CH_2), 4.18 (s, 1H, CH), 7.09–7.12 (d, $J = 12$ Hz, 2H, Ar–H), 7.33 (s, 2H, NH_2), 7.90–7.92 (d, $J = 8$ Hz, 2H, Ar–H); **^{13}C NMR** (100 MHz, DMSO-d_6) δ (ppm): 27.36, 28.84, 32.34, 35.61, 50.43, 58.21, 112.81, 119.99, 129.65, 130.27, 132.68, 144.29, 158.99, 160.66, 196.23; **MS** m/z: 328 (M^+), 330 (M + 2). Elem. anal. calcd for $C_{18}H_{17}N_2ClO_2$ (%): calcd. C, 65.75; H, 5.21; N, 8.52; found: C, 65.79; H, 5.25; N, 8.55.

2.3.5 | 2-Amino-4-(4-fluorophenyl)-5,6,7,8-tetrahydro-7,7-dimethyl-5-oxo-4*H*-chromene-3-carbonitrile

White solid (yield: 96%); m.p.: 190–192°C; **IR** (KBr, cm^{-1}): 3361 and 3325 (NH_2), 2189 (CN), 1682 (C=O); **^{1}H NMR** (400 MHz, DMSO-d_6) δ (ppm): 0.94 (s, 3H, CH_3), 1.02 (s, 3H, CH_3), 2.08–2.10 (d, $J = 8$ Hz, 2H, CH_2), 2.22–2.25 (d, $J = 12$ Hz, 2H, CH_2), 4.19 (s, 1H, CH), 6.98 (s, 2H, NH_2), 7.03–7.05 (d, $J = 8$ Hz, 2H, Ar–H), 7.40–7.42 (d, 2H, Ar–H); **^{13}C NMR** (100 MHz, DMSO-d_6) δ (ppm): 27.35, 28.85, 32.34, 35.41, 50.45, 58.53, 113.08, 115.45, 115.67, 120.19, 129.54, 129.61, 141.47, 158.98, 160.20, 163.02, 196.23; **MS** m/z: 312 (M^+). Elem. anal. calcd for $C_{18}H_{17}N_2FO_3$ (%): calcd. C, 69.22; H, 5.49; N, 8.97; found: C, 69.28; H, 5.51; N, 9.03.

2.3.6 | 7-Amino-2,3,4,5-tetrahydro-2,4-dioxo-5-p-tolyl-1*H*-pyrano[2,3-*d*]pyrimidine-6-carbonitrile

Creamish solid (yield: 94%); m.p.: 214–216°C; **IR** (KBr, cm^{-1}): 3335 and 3219 (NH_2), 2193 (CN), 1719 (C=O); **^{1}H NMR** (400 MHz, DMSO-d_6) δ (ppm): 2.25 (s, 3H, CH_3),

4.16 (s, 1H, CH), 6.95–7.17 (m, 2H, NH_2 and 4H, Ar–H), 11.06 (NH), 12.06 (NH); **^{13}C NMR** (100 MHz, DMSO-d_6) δ (ppm): 21.08, 35.66, 59.17, 78.48, 119.79, 127.44, 129.54, 136.06, 141.76, 150.20, 158.24, 159.37, 163.03; **MS** m/z: 316 (M^+), 318 (M + 2). Elem. anal. calcd for $C_{15}H_{12}N_4O_3$ (%): calcd. C, 60.81; H, 4.08; N, 18.91; found: C, 60.85; H, 4.13; N, 18.96.

2.3.7 | 7-Amino-5-(4-chlorophenyl)-2,3,4,5-tetrahydro-2,4-dioxo-1*H*-pyrano[2,3-*d*]pyrimidine-6-carbonitrile

Yellowish orange solid (yield: 93%); m.p.: 238–240°C; **IR** (KBr, cm^{-1}): 3406 and 3316 (NH_2), 2198 (CN), 1681 (C=O); **^{1}H NMR** (400 MHz, DMSO-d_6) δ (ppm): 3.39 (s, 1H, CH), 7.19 (s, 2H, NH_2), 7.30–7.32 (d, $J = 8$ Hz, 2H, Ar–H), 7.52–7.54 (d, $J = 8$ Hz, 2H, Ar–H), 9.38 (NH), 10.62 (NH); **^{13}C NMR** (100 MHz, DMSO-d_6) δ (ppm): 26.28, 55.13, 57.06, 71.61, 115.43, 128.46, 130.11, 131.65, 141.22, 152.70, 159.77, 162.88, 164.62; **MS** m/z: 316 (M^+), 318 (M + 2). Elem. anal. calcd for $C_{14}H_9N_4ClO_3$ (%): calcd. C, 53.09; H, 2.86; N, 17.69; found: C, 53.05; H, 2.90; N, 17.75.

2.3.8 | 7-Amino-2,3,4,5-tetrahydro-5-(4-hydroxyphenyl)-2,4-dioxo-1*H*-pyrano[2,3-*d*]pyrimidine-6-carbonitrile

Yellowish white solid (yield: 93%); m.p.: 290–292°C; **IR** (KBr, cm^{-1}): 3458 and 3342 (NH_2), 2225 (CN), 1609 (C=O); **^{1}H NMR** (400 MHz, DMSO-d_6) δ (ppm): 3.36 (s, 1H, CH), 7.00 (s, 2H, NH_2), 7.89–7.91 (d, $J = 8$ Hz, 2H, Ar–H), 8.32–8.34 (d, $J = 8$ Hz, 2H, Ar–H), 11.09 (NH), 11.88 (NH); **^{13}C NMR** (100 MHz, DMSO-d_6) δ (ppm): 34.85, 59.72, 75.25, 115.39, 117.30, 127.61, 134.72, 150.02, 154.04, 160.73, 161.86, 164.75; **MS** m/z: 298 (M^+). Elem. anal. calcd for $C_{14}H_{10}N_4O_4$ (%): calcd. C, 56.38; H, 3.38; N, 18.78; found: C, 56.42; H, 3.43; N, 18.83.

2.3.9 | 7-Amino-2,3,4,5-tetrahydro-5-(4-hydroxy-3-methoxyphenyl)-2,4-dioxo-1*H*-pyrano[2,3-*d*]pyrimidine-6-carbonitrile

Turmeric yellow solid (yield: 94%); m.p.: 300–302°C; **IR** (KBr, cm^{-1}): 3449 and 3305 (NH_2), 2198 (CN), 1678 (C=O); **^{1}H NMR** (400 MHz, DMSO-d_6) δ (ppm): 3.72 (s, 3H, OCH_3), 3.82 (s, 1H, CH), 6.66–6.73 (m, 3H, Ar–H), 7.03 (s, 2H, NH_2), 10.56 (NH), 11.26 (NH); **^{13}C NMR** (100 MHz, DMSO-d_6) δ (ppm): 35.67, 56.12, 59.76, 89.32, 115.82, 118.49, 119.89, 124.71, 133.06, 145.89, 147.66, 152.53, 153.56, 163.02, 164.71; **MS** m/z: 328 (M^+). Elem. anal. calcd for $C_{15}H_{12}N_4O_5$ (%): calcd. C, 54.88; H, 3.68; N, 17.07; found: C, 54.93; H, 3.72; N, 17.12.

2.3.10 | 7-Amino-5-(3-ethoxy-4-hydroxyphenyl)-2,3,4,5-tetrahydro-2,4-dioxo-1*H*-pyrano[2,3-*d*]pyrimidine-6-carbonitrile

Mustard yellow solid (yield: 95%); m.p.: 314–316°C; **IR** (KBr, cm^{-1}): 3535 and 3356 (NH_2), 2198 (CN), 1700 (C=O); **^{1}H NMR** (400 MHz, DMSO-d_6) δ (ppm): 1.34 (t, 3H, CH_3), 3.36 (s, 1H, CH), 4.01–4.10 (m, 2H, CH_2), 6.89–6.91 (m, 3H, Ar–H), 7.00 (s, 2H, NH_2), 11.14 (NH), 11.27 (NH); **^{13}C NMR** (100 MHz, DMSO-d_6) δ (ppm): 15.00, 64.23, 64.40, 75.43, 116.70, 119.35, 124.70, 128.18, 133.14, 146.59, 147.55, 150.75, 156.45, 163.04, 164.71; **MS** m/z: 342 (M^+). Elem. anal. calcd for $C_{16}H_{14}N_4O_5$ (%): calcd. C, 56.14; H, 4.12; N, 16.37; found: C, 56.20; H, 4.15; N, 16.39.

3 | RESULTS AND DISCUSSION

The catalyst WELPSA was prepared using the lemon peel collected from local lemon juice fruit factory. The peel (segregated into lemon, sweet lemon, and Kaffir lime peels) was washed cleanly with distilled water, shade-dried, and burned to obtain lemon peel ash (LPA), sweet lemon peel ash (SLPA), and Kaffir lime peel ash (KLPA). The ash was then soaked in distilled water for about 2 h, and resultant extract was filtered and collected as WELPSA (lemon) (Figure 1). We have employed scanning electron microscopy (SEM-EDX) technique to study the morphology and elemental constitution of LPA, SLPA, and KLPA (Figures 2 and 3). The composition of LPA as analyzed by EDX revealed the distribution of oxides of K, Na, Ca, and Mg in higher concentrations (please refer Table S2 for EDX spectrum).

3.1 | Determination of Na, K, Ca, and Mg in WELPSA by atom absorption spectrometry

Atomic absorption spectrometry (AAS) was used to determine the concentration of Na, K, Ca, and Mg present in WELPSA (in terms of μg/ml) that has been utilized to synthesize the title compounds. The standard solutions of sodium, potassium, calcium, and magnesium were diluted to four different concentrations and measured by using AAS Na, K, Ca, and Mg hollow cathode lamp at a wavelength of 589.0, 766.5, 422.7, and 285.2 nm,

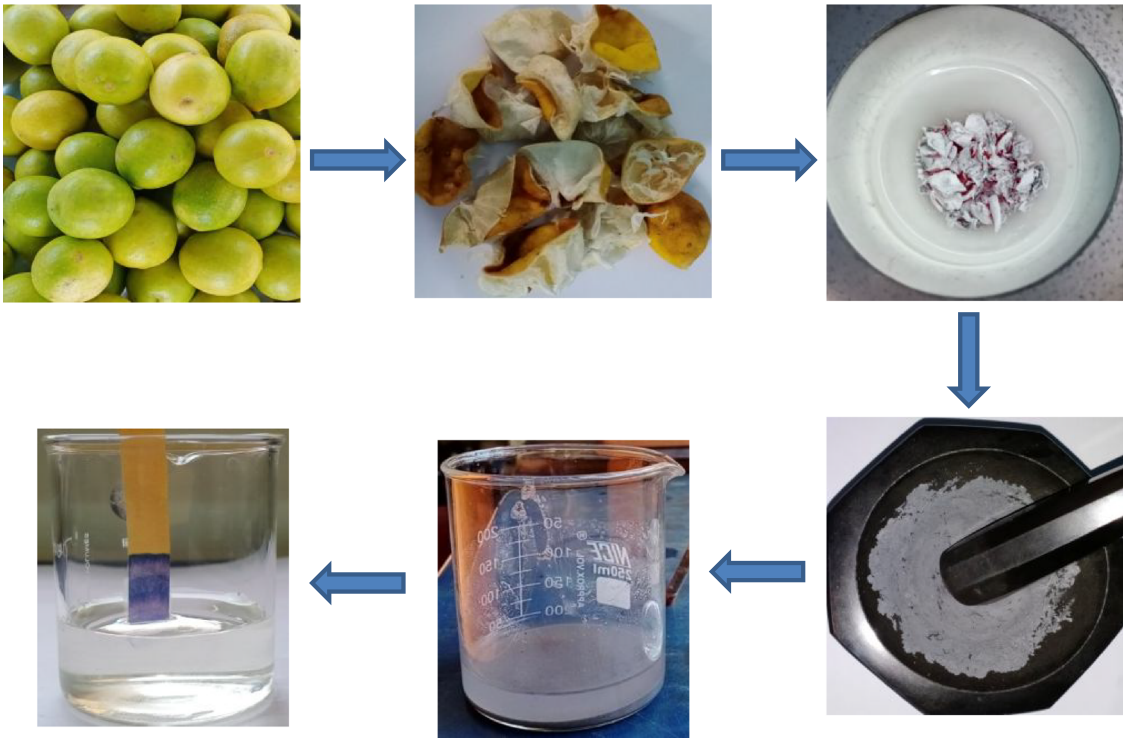

FIGURE 1 Preparation of WELPSA

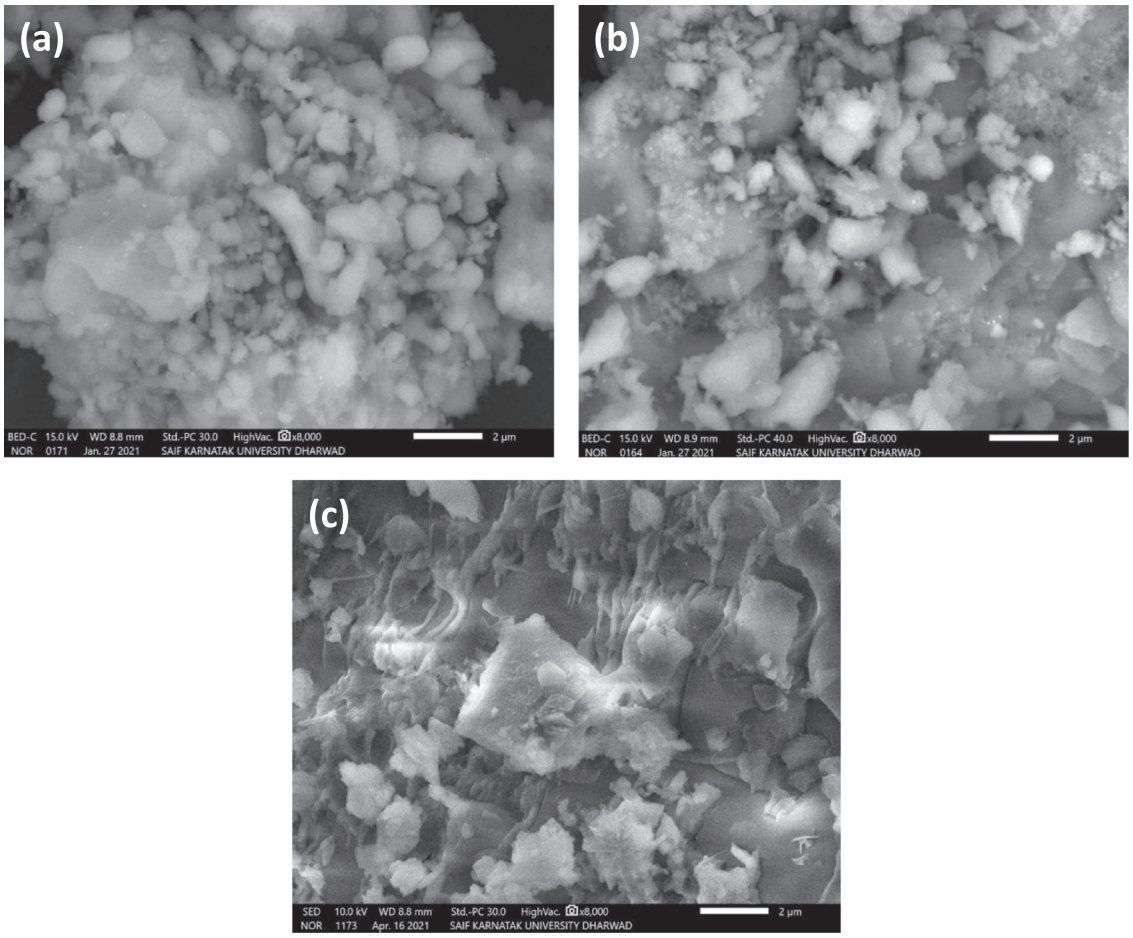

FIGURE 2 SEM images of LPA for WELPSA (a), SLPA for WESLPSA (b), and KLPA for WEKLPSA (c)

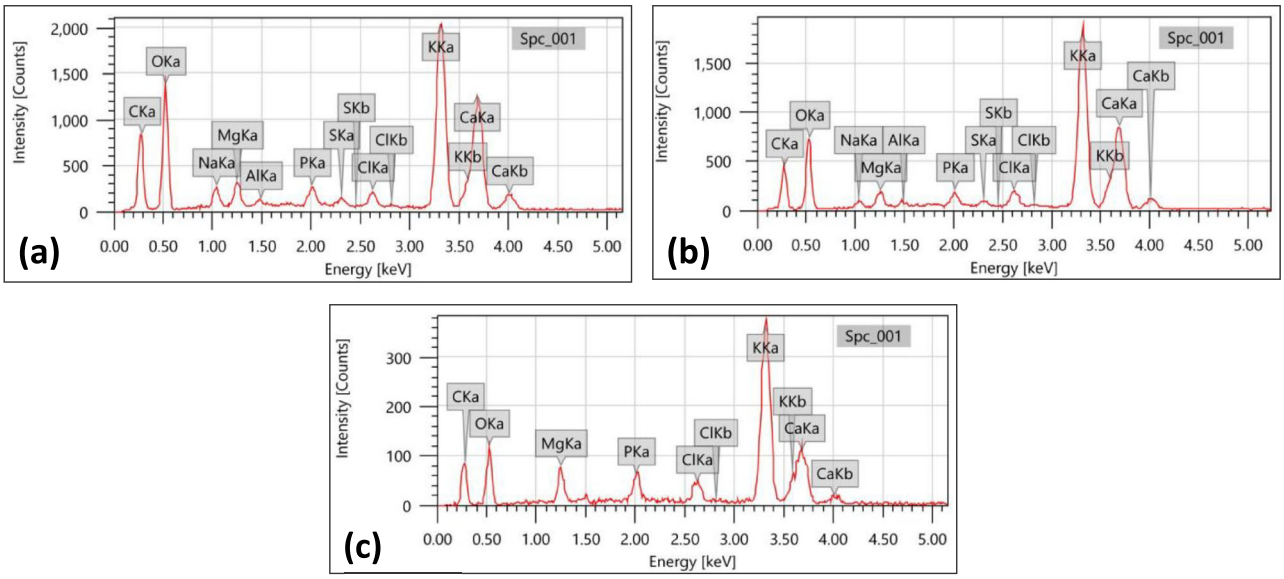

FIGURE 3 EDX spectrum of WELPSA LPA for WELPSA (a), SLPA for WESLPSA (b), and KLPA for WEKLPSA (c)

TABLE 2 Results of determination of concentrations of metal cations in WELPSA

Atom	Wave length λ_{max}	Absorbance au	Concentration µg/ml
Sodium	589.00	0.107	0.35
Potassium	766.5	1.004	0.87
Calcium	422.70	0.082	0.45
Magnesium	285.2	0.0002	0.25

TABLE 3 Optimization of reaction conditions for the compound **5a** at room temperature

Entry	Catalyst Volume (mL)	Solvent	Time (h)	Yield (%)
1	3	DMF	20	15
2	3	Acetone	16	32
3	3	DMSO	15	28
4	3	Ethanol	14	70
5	3	Methanol	15	70
6	3	Ethanol:H_2O (1:1)	12	78
7	3	THF:H_2O (1:1)	14	65
8	3	DCM	13	68
9	3	Acetonitrile	13	56
10	3	Dioxane:H_2O (1:1)	17	68
11	3	Ethanol:H_2O (1:2)	12	80
12	3	PEG-400	18	70
13	3	Ethanol:H_2O (2:1)	17	72
14	**3**	**H_2O**	**12**	**88**
15	3	Toluene	15	35

respectively, using air acetylene flame (please refer to Supporting Information for preparation method and calibration). Determination of linearity of each series standard solutions of sodium, potassium, magnesium, and calcium was obtained by measuring the absorbance of each concentration of standard solutions at their each wavelength. Linearity data are given in the Supporting Information. Absorbance was obtained from AAS according to the wavelength of each atom. Linearity data for standard sodium, potassium, magnesium, and calcium followed by calculation of the regression line equation were done with $Y = (a + bX)$, where Y is absorbance, X is concentration, a is intercept, and b is slope. The value of the coefficient of correlation (r) and coefficient of determination (r^2) calculated for sodium, potassium, magnesium, and calcium has been given in graph, which indicates linear correlation and linear determination between X (concentration) and Y (absorbance).[40] The concentration of Na, K, Ca, and Mg in WELPSA was then established by regression line equation obtained from the determination of linearity standard series solution of each atom. Results of determination of the Na, K, Ca, and Mg are listed in Table 2.

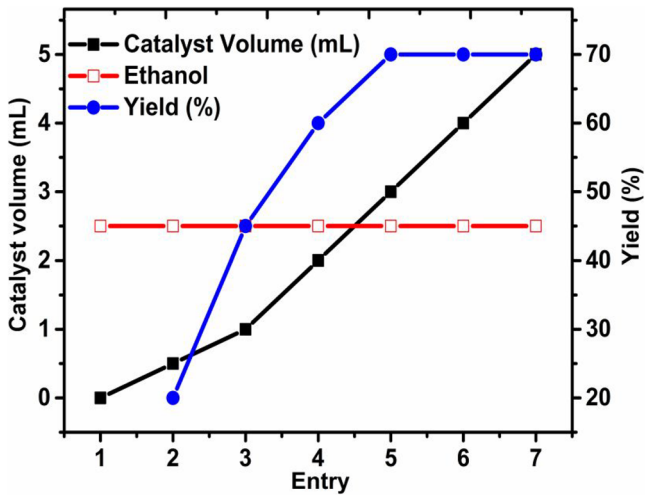

FIGURE 4 Optimization of the catalyst

The acquired results of EDX and pH clearly indicate that the oxides produced from lemon peel on thermal treatment get converted to corresponding hydroxides when soaked in water and become highly alkaline. Thus, WELPSA that acts as Lewis base is an efficient catalytic medium for the synthesis of tetrahydrobenzo[*b*]pyrans **5a–j** and pyrano[2,3-*d*]pyrimidinones **6k–t**. To begin with, we set up a three-component reaction of benzaldehyde, malononitrile, and dimedone in the presence of WELPSA (3.00 ml) and to which ethanol (5.00 ml) was added and stirred at room temperature for about 14 h. The resultant yield (70%) of the product was not satisfactory. Hence, aiming to intensify the yield, miscellaneous prerequisite conditions have been employed to optimize the reaction as notified in Figure 4 and Table 3.

In order to optimize the reaction conditions, initially we examined the minimum volume of catalyst at which the maximum yield can be furnished by carrying out the reaction of benzaldehyde, malononitrile, and dimedone

TABLE 4 Optimization of reaction conditions with different methods to furnish compound **5a**

Method	Time	Yield (%)
Grinding	4 h	70
Conventional heating	6 h	88
Room temperature	10 h	88
Microwave	3 min	96

TABLE 5 Comparison of WELPSA with identical reaction conditions in presence of analogous catalysts to furnish the compound **5a** at room temperature

Entry no.	Catalyst	Solvent	Yield (%)
1	-	H_2O	Trace
2	Na_2CO_3	H_2O	80
3	K_2CO_3	H_2O	78
4	$CaCO_3$	H_2O	Trace
5	$MgCO_3$	H_2O	Trace
6	**WELPSA**	**H_2O**	**88**

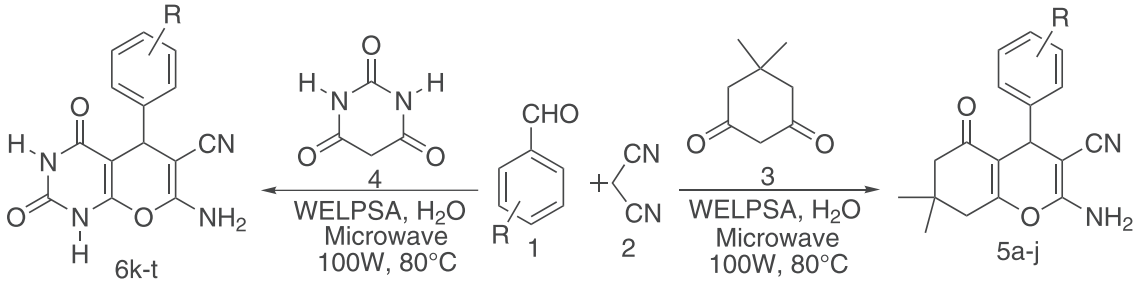

SCHEME 1 Strategic depiction to synthesize tetrahydrobenzo[*b*]pyrans **5a–j** and pyrano[2,3-*d*]pyrimidinones **6k–t**

TABLE 6 Synthesized library of compounds and their yields

Entry	Aldehyde	Product	Conventional		Microwave	
			Time (h)	Yield (%)	Time (min)	Yield (%)
5a		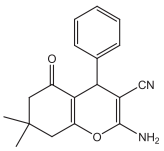	10	88	3	96
5b	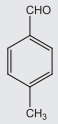	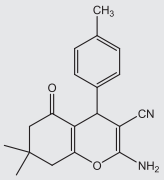	9	85	3	95
5c	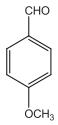	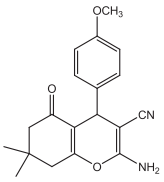	12	86	4	95
5d	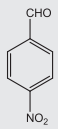	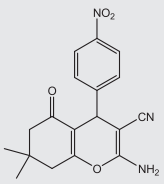	10	85	3	96
5e	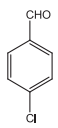	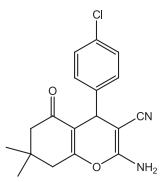	11	88	4	95
5f	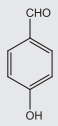	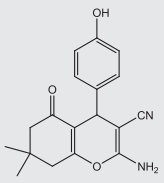	10	86	4	96

(Continues)

TABLE 6 (Continued)

Entry	Aldehyde	Product	Conventional		Microwave	
			Time (h)	Yield (%)	Time (min)	Yield (%)
5g	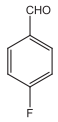	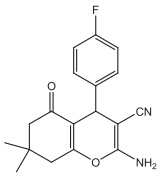	9	85	3	96
5h	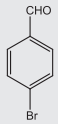	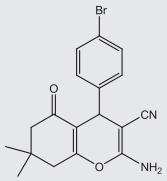	10	85	4	96
5i	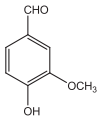	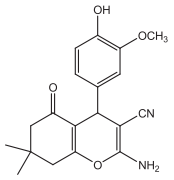	9	86	4	94
5j	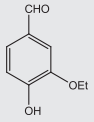	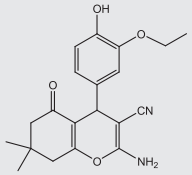	10	85	3	93
6k		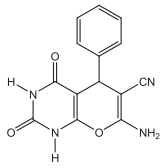	9	86	2	95
6l	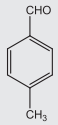	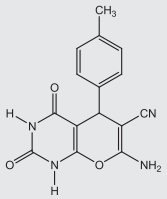	10	85	3	94

TABLE 6 (Continued)

Entry	Aldehyde	Product	Conventional		Microwave	
			Time (h)	Yield (%)	Time (min)	Yield (%)
6m	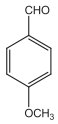	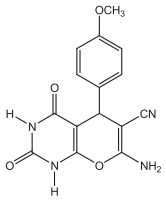	12	86	3	95
6n	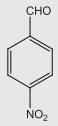	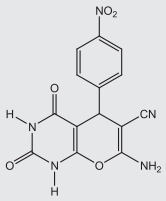	9	86	4	93
6o	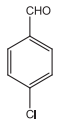	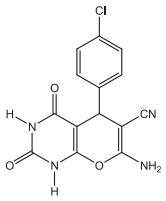	9	85	3	93
6p	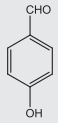	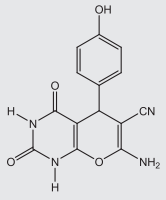	10	84	4	94
6q	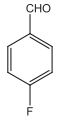	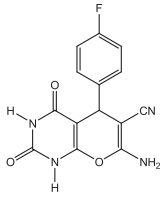	9	86	4	95
6r	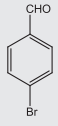		10	84	3	96

(Continues)

TABLE 6 (Continued)

Entry	Aldehyde	Product	Conventional		Microwave	
			Time (h)	Yield (%)	Time (min)	Yield (%)
		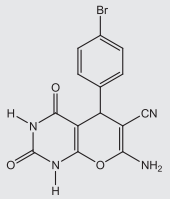				
6s	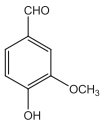	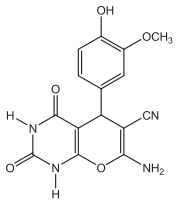	9	85	3	94
6t	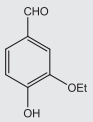	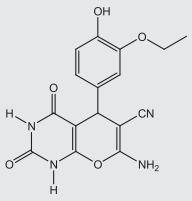	10	85	4	95

in ethanol at room temperature. We explored indiscernible reaction in diverse catalyst ratios and ended up with superior yield when the volume of the catalyst is 3.00 ml (Figure 4, Entry 5). Further increase in the catalytic ratio could not intensify the yield to any predominant extent. Currently, we perceived the catalytic amount required to obtain the title compounds **5a–j and 6k–t** (Scheme 1).

Diverse prerequisite conditions have been employed to optimize the yields in order to procure final compounds (Table 3). Initially, the reaction mixture was enabled to stir in presence of dimethylformamide (DMF), and the reaction accomplished with very poor yield (Table 3, Entry 1). When acetone and DMSO were used as solvents, no significant improvisation in the yield was observed as the same way that of DMF (Table 3, Entries 2 and 3). Emergence of moderate yield was perceived when dry methanol was used as a solvent (Table 3, Entry 5). After having carried out the reaction in aqueous ethanol (Table 3, Entry 6), which furnished with refined yield

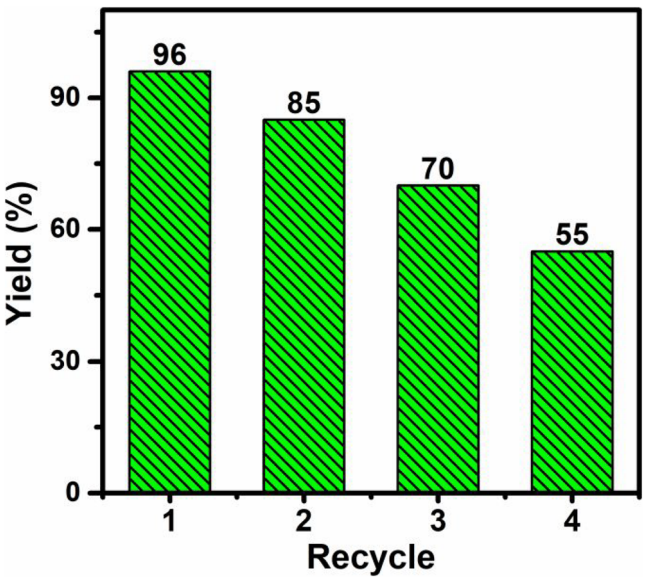

FIGURE 5 WELPSA recyclability

substantiated an overabundance of water. We assessed the identical reaction in diverse solvent systems such as THF:H_2O (1:1) (Table 3, Entry 7), dichloromethane (DCM) (Table 3, Entry 8), acetonitrile (Table 3, Entry 9), and dioxane:H_2O (1:1) (Table 3, Entry 10). An increase in the reaction yield was noticed when the ratio of H_2O was duplicated (Table 3, Entry 11). Further trial of the reaction with PEG-400 ended up with moderate yield (Table 3, Entry 12). Duplication of the ratio of ethanol furnished the final product with diminished yield (Table 3, Entry 13). Ultimately, the fruitfulness of H_2O in this protocol was ascertained. Conclusively, we comprehend that the reaction pursued more dexterously when the reaction was implemented in the subsistence of catalyst (3.00 ml) in H_2O as solvent at room temperature stimulating remarkable yield of the desired compound. In view of these peerless reaction circumstances, compound **5a** was segregated with 88% of yield (Table 3, Entry 14). Formerly revealed reaction conditions with various solvents resulted in moderate yields with extended time. Further use of other solvents did not enhance the yield to any eminent extent (Table 3, Entry 15). At this precise moment, we embraced (perceived) the relevance of H_2O in the synthesis of pyran derivatives **5a–t**.

Such an organization of catalyst and the solvent was benefited to furnish the compound **5a** underneath different methods like grinding, conventional heating, stirring

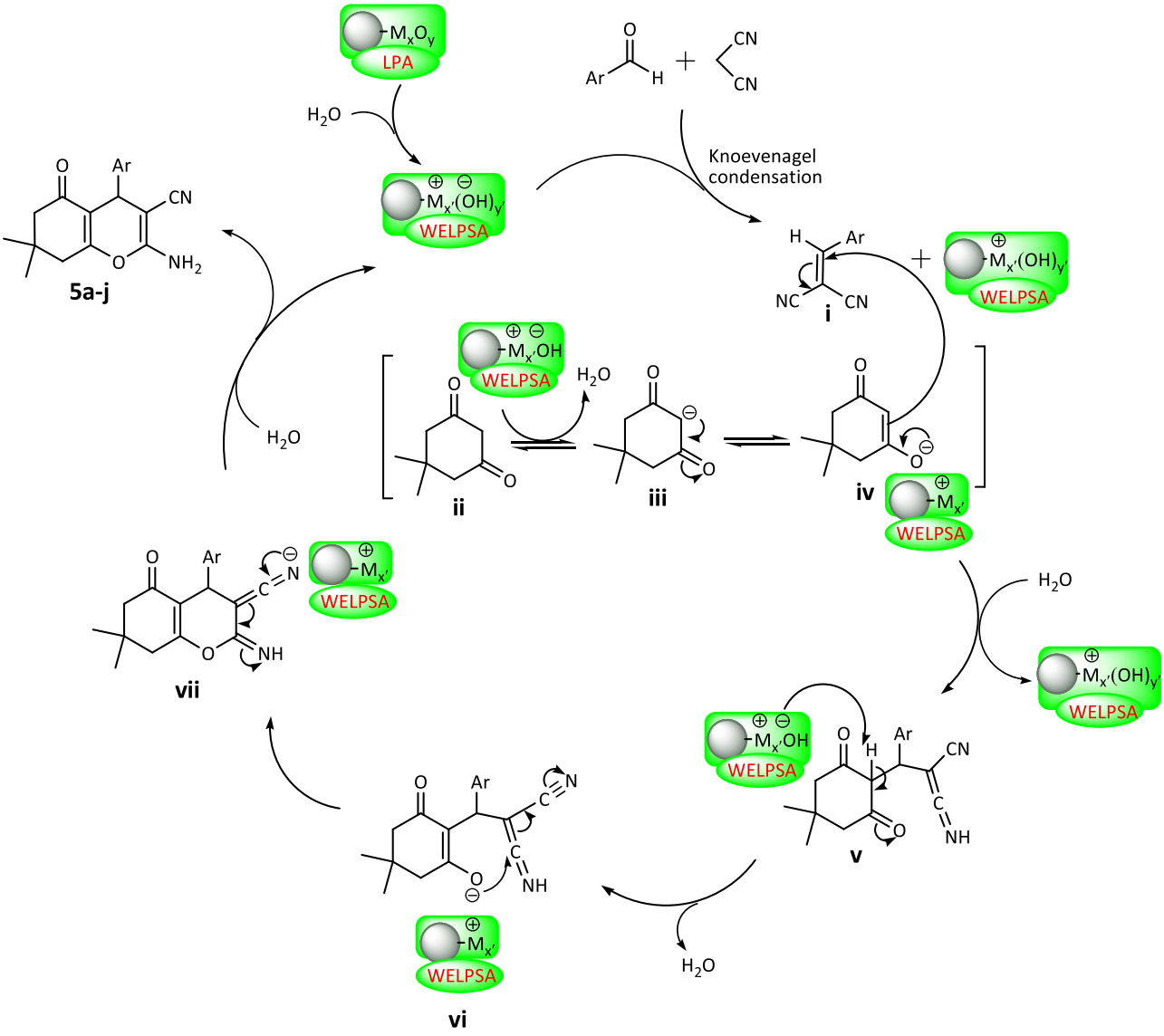

M_xO_y (x = 2, y = 1, when M = Na, K and x = 1, y = 1, when M = Ca and Mg)
$M_{x'}(OH)_{y'}$ (x' = 1 and y' = 1, If M = Na, K and x' = 1, y' = 2, when M = Ca and Mg)

SCHEME 2 Plausible mechanism for the emergence of tetrahydrobenzo[*b*]pyrans **5a–j**

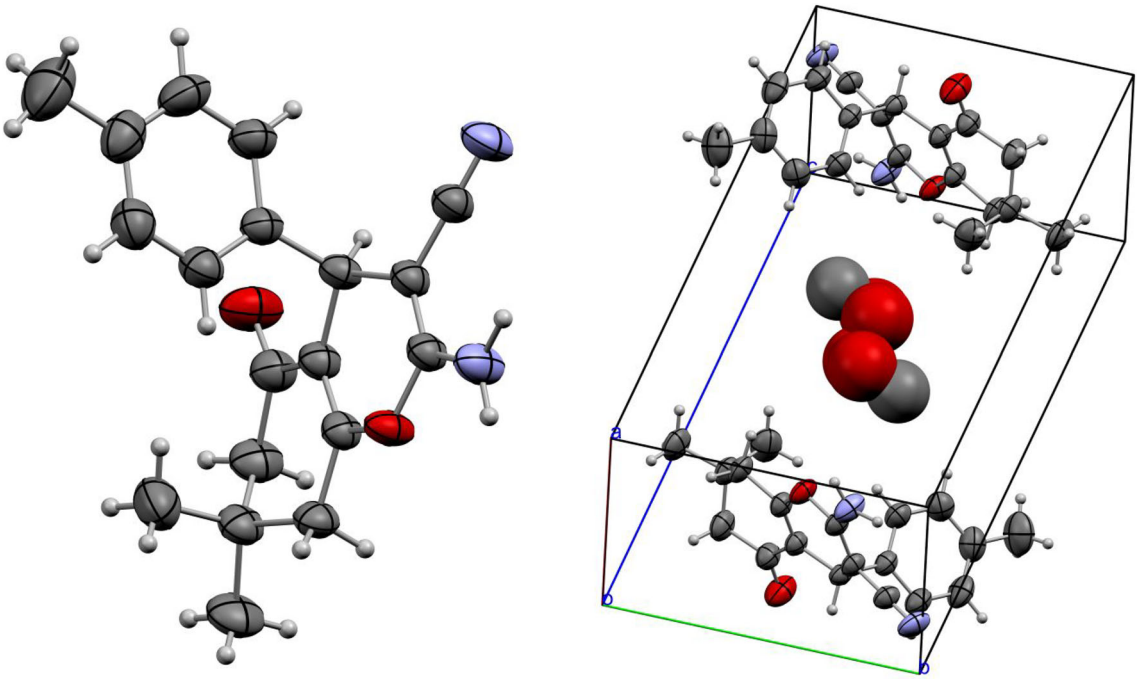

FIGURE 6 ORTEP projection and packing diagram of compound **5b**

at customary temperature, and microwave irradiation. In all the methods, the reaction was accomplished with acceptable yields by means of longer time duration apart from microwave method, which astonished us with 96% yield in 3 min. Microwave irradiation method endeavored augmented yields instantaneously in comparison with the conventional method (Table 4).

Because the aqueous solutions of carbonates of alkali and alkaline earth metals are also basic in nature, we further planned to carryout similar reaction in the presence of Na_2CO_3, K_2CO_3, $CaCO_3$, and $MgCO_3$ as catalysts in order to create identical reaction condition and compared the same with WELPSA. The reaction proceeded with the formation of desired product only in the presence of Na_2CO_3 and K_2CO_3 as their aqueous solutions are basic, and as per the proposed mechanism, the reaction occurred when the oxides are converted into hydroxides of base. However, $CaCO_3$ and $MgCO_3$ are sparingly soluble or insoluble; a trace amount of the product was observed (Table 5).

An array of structurally divergent tetrahydrobenzo[*b*]pyrans **5a–j** and pyrano[2,3-*d*]pyrimidinones **6k–t** were accomplished in adequate yields, making the use of aforesaid provisions and are embodied in Table 6. WELPSA being generated from agro-waste acted as a superior catalyst compared with all other with escalated yield. The other two catalysts WESLPSA and WEKLPSA obtained from the agro-waste were also observed to be better catalysts to synthesize the pyran derivatives. However, there was no significant difference observed in the reaction catalyzed by WELPSA, WESLPSA, and WEKLPSA, and hence, we synthesized library of these compounds utilizing WELPSA only.

3.2 | Catalyst reusability

The reusability of catalyst WELPSA was assessed for the synthesis of compound **5a** considering it as model reaction under the optimized conditions. The catalyst was secluded by simple filtration as filtrate once the reaction was accomplished and the same filtrate was used in repeated cycles to obtain compound **5a** under similar reaction conditions. Surprisingly, the WELPSA catalyst can be recycled not lesser than four times (Figure 5). This adds up as an auxiliary evident for supremacy of the present protocol (Table 3, Entry 15), which has numerous advantages like greener, economic, and simpler reaction setup and product isolation superior to known methods for the synthesis of tetrahydrobenzo[*b*]pyrans **5a–j** and pyrano[2,3-*d*]pyrimidinones **6k–t**.

3.3 | Plausible mechanism

Formation of tetrahydrobenzo[*b*]pyrans **5a–j** may be shown by a plausible mechanism involving the catalytic cycle as depicted in Scheme 2. The oxides in the LPA are

converted into the corresponding hydroxides to form WELPSA when soaked in water. WELPSA catalyzes the reaction of aldehyde **1** and malononitrile **2** into benzylidene malononitrile ***i***, which further experiences the nucleophilic attack by enolate anion ***iv*** generated from the dimedone **3** under the influence of another

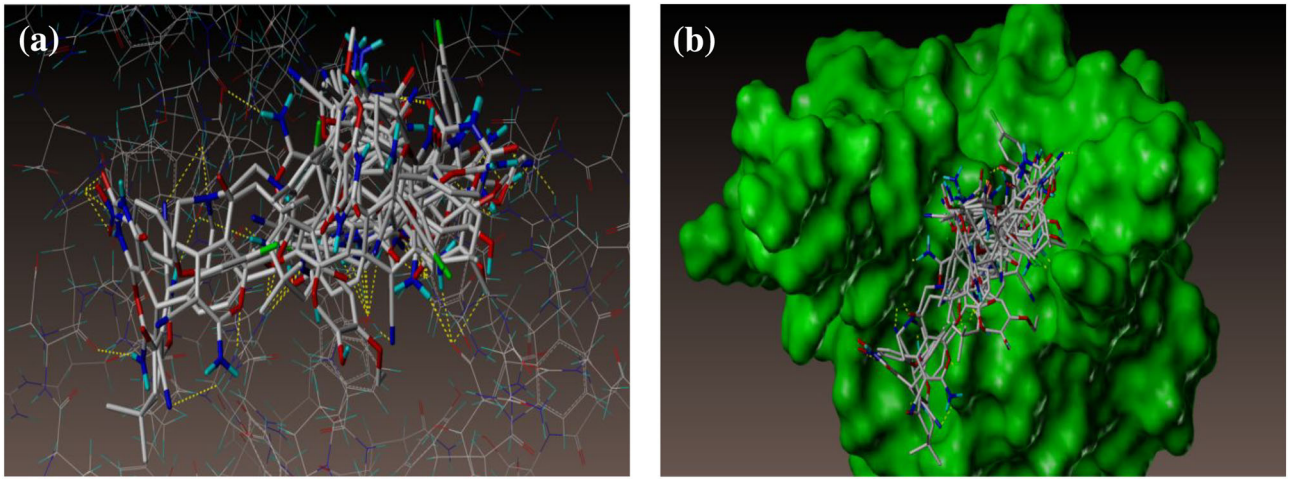

FIGURE 7 Docked view of all the compounds at the active site of the enzyme PDB ID: 6M3M

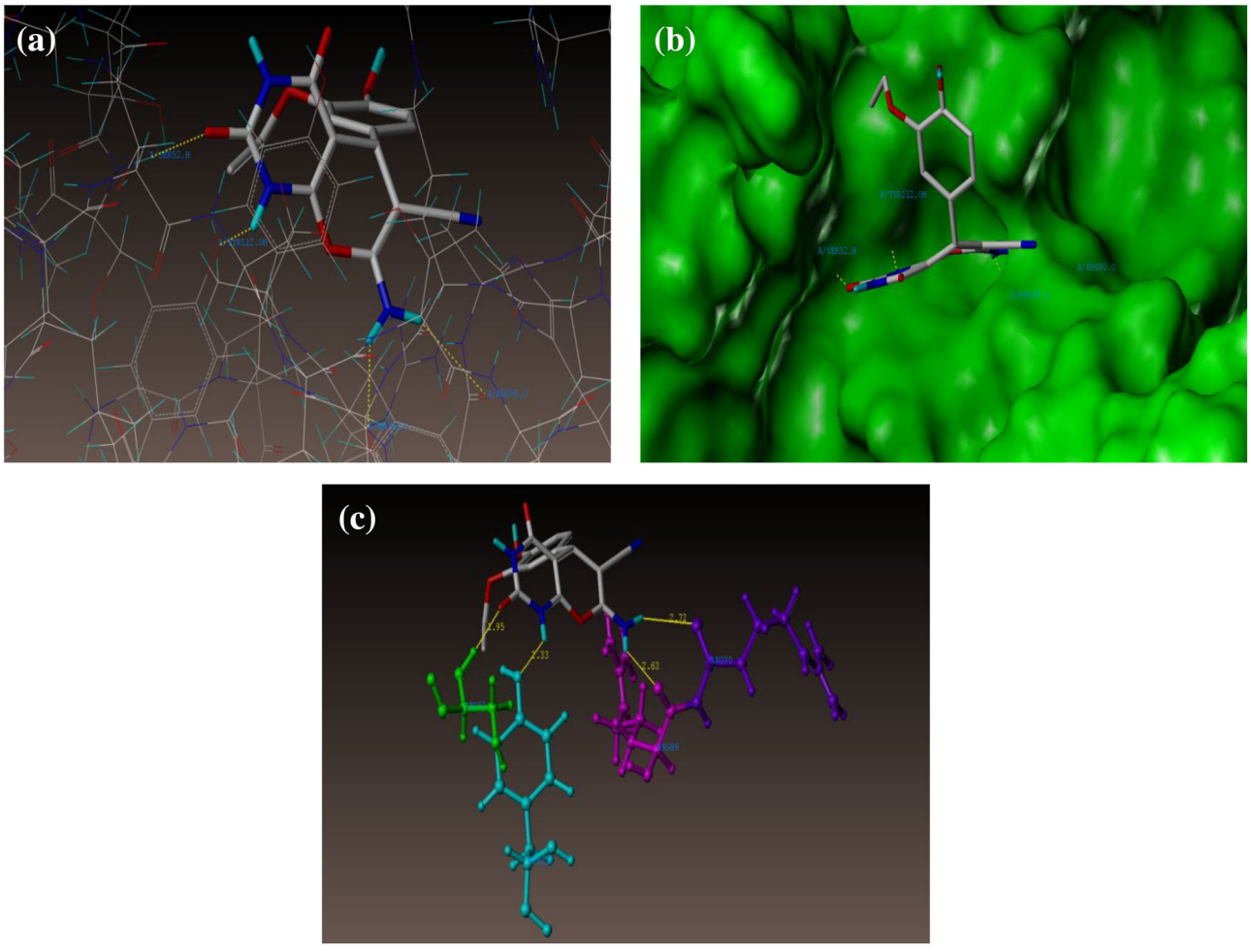

FIGURE 8 Docked view of compound **6t** at the active site of the enzyme PDB: 6M3M

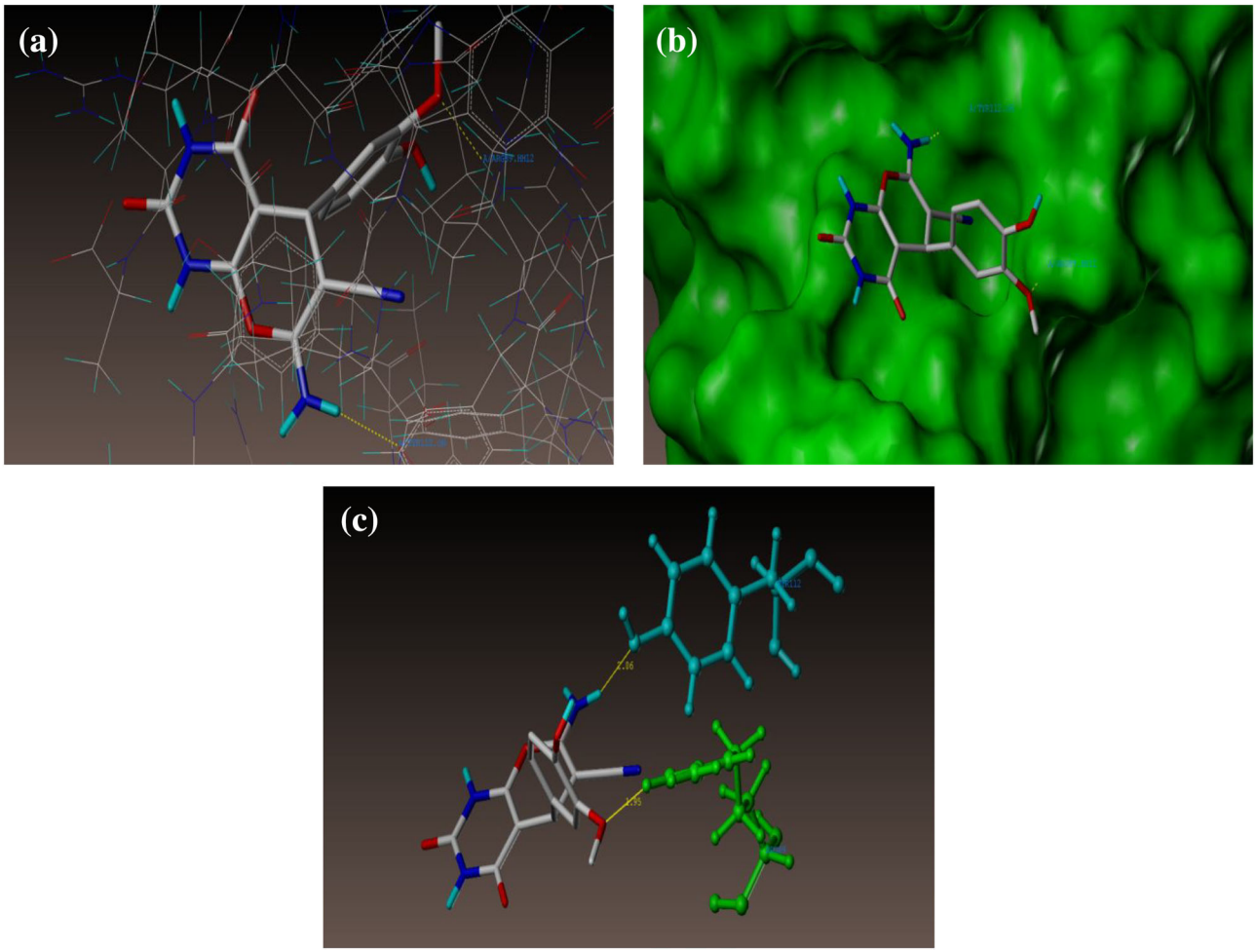

FIGURE 9 Docked view of compound **6s** at the active site of the enzyme PDB: 6M3M

molecule of WELPSA to form the intermediate ***v***. WELPSA removes the acidic proton from intermediate ***v*** to form an adduct ***vi***. Intramolecular nucleophilic attack in the adduct ***vi*** leads to cyclization, and another adduct ***vii*** is formed, which in the presence of water forms the compound **5a–j**. During this step, WELPSA is regenerated and plays similar role in such cycles. Also, the pyrano[2,3-*d*]pyrimidinones **6k–t** are obtained through the similar mechanism.

A single crystal for the compound **5b** has been grown by slow evaporation method. The structural orientation of as-grown **5b** compound was found to be a triclinic crystal system with *P*-1 space group with the unit cell parameters a = 8.1090(5) Å, b = 9.2656(8) Å, c = 13.7415 (10) Å, α = 85.750(7)°, β = 79.754(6)°, and γ = 78.155 (6)°.[41–43] The ORTEP of the molecule with thermal ellipsoids drawn at 50% probability and packing of the molecules are shown in Figure 6. Detailed crystal data are provided as Table S1.

4 | MOLECULAR DOCKING STUDIES

The CoV-N protein, a RNA binding protein, has many functions such as transcription and translation in RNA. It also plays numerous decisive functions in molding helical ribonucleoproteins throughout regulating viral RNA synthesis, packaging of viral genome, and adapting infected cell metabolism.[44,45] Hence, viral nucleoplasmid protein is a potential antiviral drug target for inhibiting the RNA transcript and translation, thus inhibiting the virus. Hence, compounds were docked on the crystal structure of SARS-CoV-2 nucleocapsid protein N-terminal RNA binding domain (PDB ID 6M3M, 2.70 Å x-ray diffraction) using the Surflex-Dock program of sybyl-X 2.0 software as a means to elucidate the mechanism and detailed intermolecular interactions. All the inhibitors along with the standard (6-chloro-7-((2-morpholinoethyl)amino)quinoline-5,8-dione) were

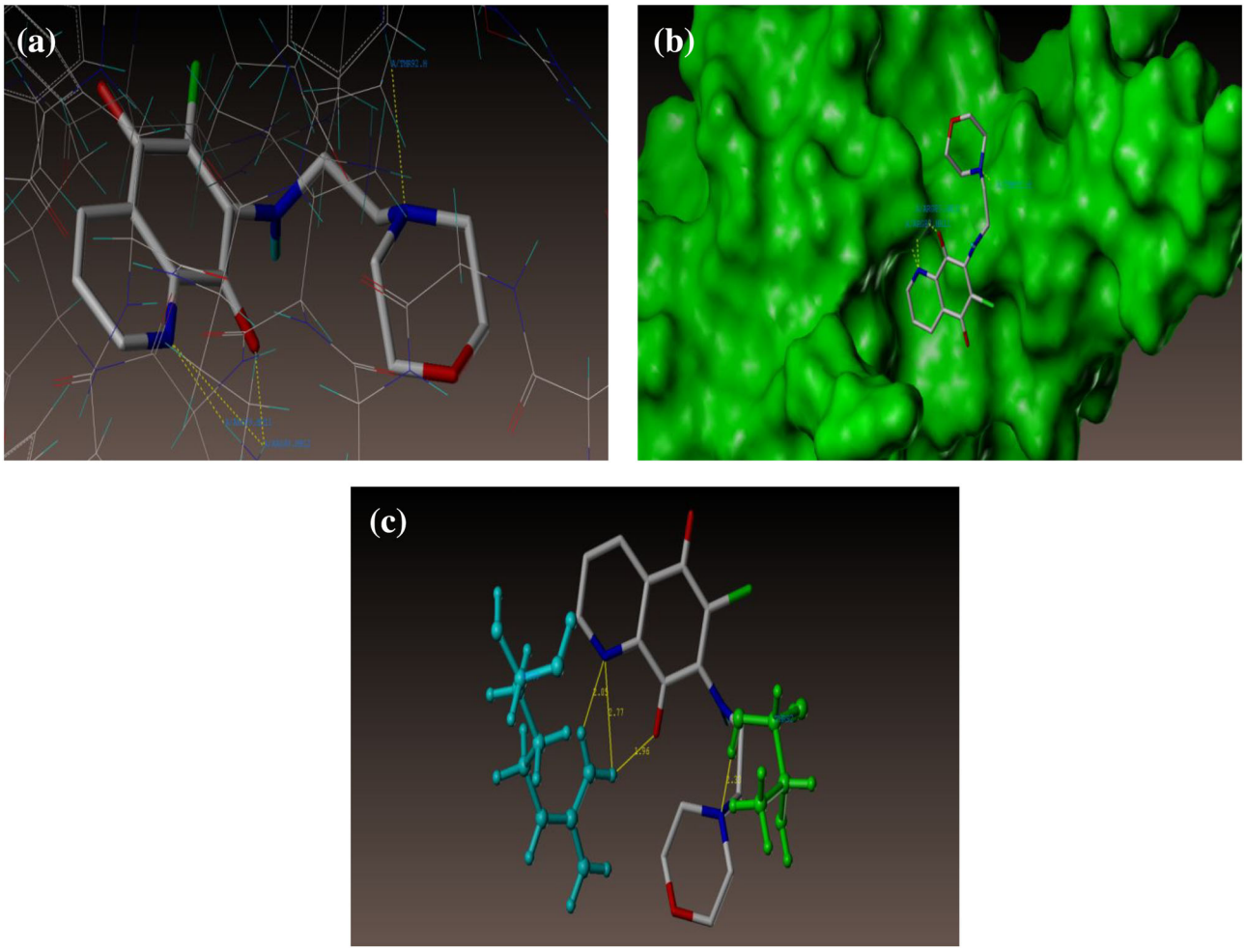

FIGURE 10 Docked view of standard compound at the active site of the enzyme PDB: 6M3M

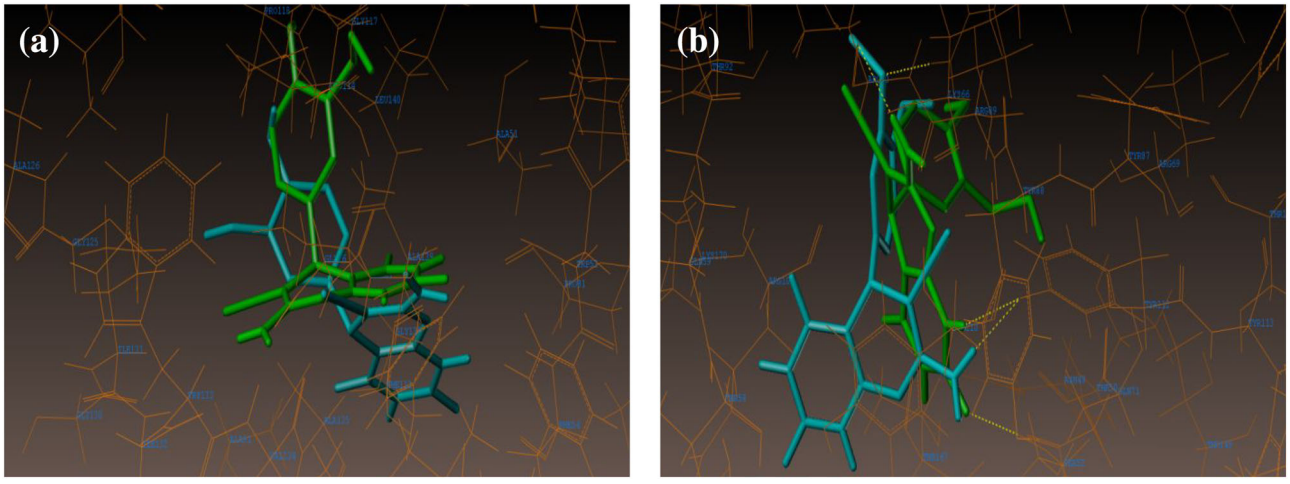

FIGURE 11 (a) Hydrophobic amino acids surrounded to compounds **6t** (green color) and **6s** (cyan color). (b) Hydrophilic amino acids surrounded to compounds **6t** and **6s**

docked into the active site of protein as depicted in Figure 7a,b. The predicted binding energies of the compounds are tabulized in Table 7. The docking study disclosed that all the compounds have displayed very good docking score against the protein.

Figure 8a–c exhibits the compound **6t** fabricating four hydrogen bonding interactions at the energetic spot of the enzyme (PDB ID: 6M3M), among which two interactions were due to hydrogen atoms of amino group present on the 7th position of pyronopyrimidine ring with oxygen atoms of ARG89 and ARG90 (H------O-ARG89, 2.635 Å; H------O-ARG90, 2.72 Å), oxygen atom present at the 2nd position of pyranopyrimidine ring forms hydrogen bonding interface with hydrogen atom of SER52 (O------H-SER52, 1.95 Å), and residual hydrogen bonding interaction was from the hydrogen atom of NH at 1st position of pyrano ring with oxygen atom of TYR112 (H-----O-TYR112, 2.33 Å).

As outlined in Figure 9a–c, two hydrogen bonding interactions emerged at the active site of the enzyme owing to compound **6s** among which one due to the oxygen atom of methoxy group present on the 3rd position of phenyl ring with hydrogen atom of ARG89 (O------H-ARG89, 1.95 Å) and another interaction was observed from the hydrogen atom of amino group present on the 7th position of pyranopyrimidine ring with oxygen atom of TYR112 (H-----O-TYR112, 2.05 Å).

The docked view of standard compound (6-chloro-7-((2-morpholinoethyl)amino)quinoline-5,8-dione) at the active site of the enzyme (PDB ID: 6M3M) makes four hydrogen bonding interactions as depicted in Figure 10a–c, among which two interactions were of nitrogen atom present on the 1st position of quinoline ring with hydrogen atoms of ARG89 (N------H-ARG89, 2.05 Å; 2.77 Å), oxygen atom present at the 8th position of quinoline ring composes an interaction with hydrogen atom of ARG89 (O------H-ARG89, 1.96 Å), and residual one interaction was by virtue of nitrogen atom of morpholine ring with hydrogen of THR92 (N-----H-THR92, 2.33 Å). Figure 11a,b signifies the hydrophobic and hydrophilic amino acids surrounded to the studied compounds **6t** and **6s**.

The consensus score in the range 2.47–4.63 implicates that docking study was optimistic, indicating the summary of all forces of interaction between ligands and the protein. The docked postures unveiled that the compounds that have been studied manifested identical interaction with amino acid residue (ARG89) as that of

TABLE 7 Surflex docking score (kcal/mol) of the derivatives (PDB: 6M3M)

Compounds	C score[a]	Crash score[b]	Polar score[c]	D score[d]	PMF score[e]	G score[f]	Chem score[g]
Standard	4.63	−0.96	2.35	−77.045	−16.464	56.781	−20.449
5j	4.20	−1.77	1.52	−87.274	−41.520	−173.307	−20.901
5i	4.20	−1.78	1.32	−87.722	−40.355	−169.099	−20.619
5c	4.15	−1.21	0.00	−79.879	−25.823	−180.695	−16.327
6t	3.41	−0.85	1.07	−75.076	−72.023	−142.250	−10.396
5f	3.35	−0.72	1.06	−59.901	−52.284	−124.598	−18.614
6m	3.19	−0.34	2.28	−52.992	−51.624	−94.862	−15.137
6n	3.11	−0.56	2.90	−62.976	−38.091	−118.028	−17.606
6s	2.82	−0.38	2.24	−60.489	−48.862	−83.674	−13.883
6k	2.55	−0.19	2.33	−45.733	−45.110	−81.876	−14.852
6q	2.53	−0.18	2.32	−46.210	−46.136	−82.774	−14.903
6o	2.52	−1.13	1.62	−64.990	−26.241	−133.274	−11.213
5d	2.47	−0.37	3.32	−37.905	−28.625	−72.868	−15.046

[a]CScore (consensus score): This is an integration of the number of popular scoring functions for assessing the affinity of synthesized compounds docked into the active site of the protein, and this is the total score.
[b]Crash score: It indicates the unsuitable penetration into the docking pocket. Crash scores nearer to 0 are favorable. The negative numbers illustrate the penetration.
[c]Polar score: The polar score is a measure of polar interactions to the total score and is useful for excluding docking results that make no hydrogen bonds.
[d]D score: It reveals the charge and van der Waals interactions between the receptor and the reported compounds.
[e]PMF score: This indicates the Helmholtz free energies of interactions between the receptor and the atom pairs of the synthesized molecule or the reference compound (potential of mean force, PMF).
[f]G score: It is a measure of H-bond between the external (compound–protein) and internal (compound–compound).
[g]Chem score: This indicates the H-bonding, lipophilic contact, and rotational entropy, along with an intercept term.

TABLE 8 Comparison of different catalysts with WELPSA to synthesize **5a**

Entry	Catalyst	Solvent	Yield (%)
1	ZnONPs	EtOH: H_2O (1:1)	86[14]
2	Fe_3O_4@SiO_2@BenzIm-Fc[Cl]/$NiCl_2$	EtOH: H_2O (4:2)	95[15]
3	[H_2-DABCO][H_2PO_4]$_2$	EtOH: H_2O (2:1)	90[16]
4	RHPrBPCl nanocomposite	H_2O	90[18]
5	Glutamic acid	EtOH	90[19]
6	$CaHPO_4$	EtOH: H_2O (1:4)	91[22]
8	WELPSA	H_2O	96[a]

[a]Present work.

TABLE 9 Comparison of different catalysts with WELPSA to synthesize **6k**

Entry	Catalyst	Solvent	Yield (%)
1	[H_2-DABCO][H_2PO_4]$_2$	EtOH: H_2O (2:1)	95[16]
2	DAHP	EtOH: H_2O (1:1)	81[17]
3	*L*-Proline	EtOH: H_2O (1:1)	80[21]
4	$CaHPO_4$	EtOH: H_2O (1:4)	89[22]
5	WELPSA	H_2O	95[a]

[a]Present work.

standard. In conclusion, synthesized molecules preferentially bind to enzyme (PDB: 6M3M) in comparison with the standard (Table 7).

5 | EFFICIENCY OF WELPSA

The efficacy of catalyst WELPSA was compared with the other reported catalysts (Tables 8 and 9). Overall, the relative results revealed that the performance of WELPSA was superior in different factors like the solvent, yield, reusability of the catalyst, and yield of the final product. The use of water as solvent is the major difference among all.

6 | CONCLUSIONS

The Covid-19 outbreak by SARS-CoV-2 virus incessantly led to worldwide human infections and mortality. There is no specific viral protein-targeted therapeutics, and viral nucleoplasmid CoV-N-protein is a promising target. The design of catalyst and thus to devise a process that reduces the use and generation of hazardous substances is the need of the hour. In view of all these, a meritorious, proficient, user-friendly, and environmentally benign one-pot synthetic protocol has been flourished to elucidate the synthesis of tetrahydrobenzo[*b*]pyrans **5a–j** and pyrano[2,3-*d*]pyrimidinones **6k–t** effectually in water. In all the methods, the reaction was accomplished with acceptable yields by means of longer time duration except microwave method, which amazed us with 93%–96% yield in 3 min. The current approach manifests numerous notable advantages that include ease of preparation, handling and benignity of the catalyst, low cost, green reaction conditions, facile workup, and excellent yields (93%–96%). The docking analysis of these compounds against SARS-CoV-2 nucleoplasmid protein N-terminal RNA binding protein indicated a favorable binding, thus showing the inhibition. Comprehensively, the contemporary study may transform the approach of a chemist for the expansion of pharmaceutically important pyrans.

ACKNOWLEDGMENTS

One of the authors (ARN) is grateful to DST-KSTePS, Govt. of Karnataka, for providing the Fellowship. The authors are obliged to DST-PURSE Phase-II, SAIF, University Scientific Instrumentation Center (USIC), Karnatak University, Dharwad, and Institution of Excellence, University of Mysore, Mysore, India, for providing the UPLC-mass spectral data and facilities to conduct the experiments.

CONFLICT OF INTEREST

The authors declare no conflict of interest.

AUTHOR CONTRIBUTIONS

Aravind Nesaragi: Conceptualization; data curation; formal analysis; investigation; methodology; software;

visualization. **Ravindra R. Kamble:** Formal analysis; investigation; project administration; resources; supervision. **Swati Hoolageri:** Data curation; formal analysis; validation. **Ahmedraza Mavazzan:** Formal analysis; validation; visualization. **Suresh Madar:** Formal analysis; validation; visualization. **Ashish Anand:** Data curation; methodology; visualization. **Shrinivas Joshi:** Data curation; formal analysis; investigation; software.

DATA AVAILABILITY STATEMENT

The data that support the findings of this study are available in the Supporting Information of this article.

ORCID

Aravind R. Nesaragi https://orcid.org/0000-0002-6659-2243
Ravindra R. Kamble https://orcid.org/0000-0002-0384-655X
Swati R. Hoolageri https://orcid.org/0000-0002-1816-7496
Ahmedraza Mavazzan https://orcid.org/0000-0002-3457-2424
Suresh F. Madar https://orcid.org/0000-0002-4497-2296
Ashish Anand https://orcid.org/0000-0003-1279-4189
Shrinivas D. Joshi https://orcid.org/0000-0002-6520-806X

REFERENCES

[1] https://www.who.int/emergencies/diseases/novel-coronavirus-2019 (accessed on 5 August 2021).
[2] M. Hosseini, W. Chen, D. Xiao, C. Wang, *Precis. Clin. Med.* **2021**, *4*, 1.
[3] https://www.bbc.com/news/business-51706225 (accessed on 5 August 2021).
[4] S. Choudhary, Y. S. Malik, S. Tomar, *Front. Immunol.* **2020**, *11*, 1664.
[5] S. Kumar, P. P. Sharma, U. Shankar, D. Kumar, S. K. Joshi, L. Pena, R. Durvasula, A. Kumar, P. Kempaiah, Poonam, B. Rathi, *J. Chem. Inf. Model.* **2020**, *60*, 5754.
[6] https://www.worldometers.info/coronavirus/#news (accessed on 5 August 2021).
[7] A. Sarkar, S. Santra, S. K. Kundu, A. Hajra, G. V. Zyryanov, O. N. Chupakhin, V. N. Charushin, A. Majee, *Green Chem.* **2016**, *18*, 4475.
[8] Y. Gu, *Green Chem.* **2012**, *14*, 2091.
[9] R. Ramesh, S. Maheswari, J. G. Malecki, A. Lalitha, *Polycyclic Aromat. Compd.* **2020**, *40*, 1581.
[10] J. Zhang, H. Song, R. Cui, C. Deng, Q. A. Yousif, *J. Coord. Chem.* **2020**, *73*, 558.
[11] M. Biglari, F. Shirini, N. O. Mahmoodi, M. Zabihzadeh, M. Mashhadinezhad, *J. Mol. Struct.* **2020**, *1205*, 127652.
[12] H. A. Oskooie, M. M. Heravi, N. Karimi, M. E. Zadeh, *Synth. Commun.* **2011**, *41*, 436.
[13] T. Lohar, A. Kumbhar, M. Barge, R. Salunkhe, *J. Mol. Liq.* **2016**, *224*, 1102.
[14] R. Pourhasan-Kisomi, F. Shirini, M. Golshekan, *Appl. Organomet. Chem.* **2018**, *32*, 1.
[15] G. Brahmachari, B. Banerjee, *ACS Sustainable Chem. Eng.* **2014**, *2*, 2802.
[16] S. Khaksar, A. Rouhollahpour, S. M. Talesh, *J. Fluorine Chem.* **2012**, *141*, 11.
[17] S. K. Dangolani, F. Panahi, M. Nourisefat, A. Khalafi-Nezhad, *RSC Adv.* **2016**, *6*, 92316.
[18] M. Abdollahi-Alibeik, F. Nezampour, *React. Kinet., Mech. Catal.* **2013**, *108*, 213.
[19] D. Tahmassebi, J. A. Bryson, S. I. Binz, *Synth. Commun.* **2011**, *41*, 2701.
[20] P. Bhattacharyya, K. Pradhan, S. Paul, A. R. Das, *Tetrahedron Lett.* **2012**, *53*, 4687.
[21] R. Mohammadi, S. Esmati, M. Gholamhosseini-Nazari, R. Teimuri-Mofrad, *J. Mol. Liq.* **2019**, *275*, 523.
[22] F. Shirini, M. S. N. Langarudi, N. Daneshvar, *J. Mol. Liq.* **2017**, *234*, 268.
[23] S. Balalaie, S. Abdolmohammadi, H. R. Bijanzadeh, A. M. Amani, *Mol. Diversity* **2008**, *12*, 85.
[24] A. R. Kiasat, S. Hamid, S. J. Saghanezhad, *Nanochem Res* **2016**, *1*, 157.
[25] F. Hatamjafari, *J Chem. Health Risks.* **2016**, *6*, 133.
[26] J. Yang, S. Liu, H. Hu, S. Ren, A. Ying, *Chinese J. Chem. Eng.* **2015**, *23*, 1416.
[27] M. Bararjanian, S. Balalaie, B. Movassag, A. M. Amani, *J. Iran. Chem. Soc.* **2009**, *6*, 436.
[28] M. A. Bodaghifard, M. Solimannejad, S. Asadbegi, S. Dolatabadifarahani, *Res. Chem. Intermed.* **2016**, *42*, 1165.
[29] R. Nongrum, G. S. Nongthombam, M. Kharkongor, J. W. Star Rani, N. Rahman, C. Kathing, B. Myrboh, R. Nongkhlaw, *RSC Adv.* **2016**, *6*, 108384.
[30] D. K. Yadav, M. A. Quraishi, *J. Mater. Environ. Sci.* **2014**, *5*, 1075.
[31] J. Albadi, A. Mansournezhad, T. Sadeghi, *Res. Chem. Intermed.* **2015**, *41*, 8317.
[32] B. Sabour, M. H. Peyrovi, M. Hajimohammadi, *Res. Chem. Intermed.* **2015**, *41*, 1343.
[33] M. Pourghasemi-Lati, F. Shirini, M. Alinia-Asli, M. A. Rezvani, *Appl. Organomet. Chem.* **2018**, *32*, 1.
[34] M. A. Zolfigol, R. Ayazi-Nasrabadi, S. Baghery, *Appl. Organomet. Chem.* **2016**, *30*, 273.
[35] K. Kantharaju, S. Y. Khatavi, *ChemistrySelect* **2018**, *3*, 5016.
[36] P. B. Hiremath, K. Kamanna, *Curr. Microw. Chem.* **2019**, *6*, 30.
[37] S. Shinde, S. Damate, S. Morbale, M. Patil, S. S. Patil, *RSC Adv.* **2017**, *7*, 7315.
[38] D. Habibi, M. Nasrollahzadeh, T. A. Kamali, *Green Chem.* **2011**, *13*, 3499.
[39] S. Gulati, R. Singh, J. Sindhu, S. Sangwan, *Org. Prep. Proced. Int.* **2020**, *52*, 381.
[40] N. Nerdy, *IOP Conf. Ser. Mater. Sci. Eng.* **2018**, *288*, 012113.
[41] G. M. Sheldrick, *Acta Crystallogr. Sect. A Found. Crystallogr.* **2008**, *64*, 112.
[42] P. Van Der Sluis, A. L. Spek, *Acta Crystallogr. Sect. A.* **1990**, *46*, 194.

[43] C. F. Macrae, I. J. Bruno, J. A. Chisholm, P. R. Edgington, P. McCabe, E. Pidcock, L. Rodriguez-Monge, R. Taylor, J. Van De Streek, P. A. Wood, *J. Appl. Crystallogr.* **2008**, *41*, 466.
[44] R. S. Baric, G. W. Nelson, J. O. Fleming, R. J. Deans, J. G. Keck, N. Casteel, S. A. Stohlman, *J. Viral.* **1988**, *62*, 4280.
[45] Y. Cong, M. Ulasli, H. Schepers, M. Mauthe, P. Vkovski, F. Kriegenburg, V. Thiel, C. A. M. de Haan, F. Reggiori, *J. Viral.* **2020**, *94*, 01925.

SUPPORTING INFORMATION

Additional supporting information may be found in the online version of the article at the publisher's website.

How to cite this article: A. R. Nesaragi, R. R. Kamble, S. R. Hoolageri, A. Mavazzan, S. F. Madar, A. Anand, S. D. Joshi, *Appl Organomet Chem* **2021**, e6469. https://doi.org/10.1002/aoc.6469